Particle-In-Cell modelling of acceleration region in Hall Thruster

L Nicole, P Sarrailh, M Villemant, L Garrigues, C Boniface

Particle-In-Cell modelling of acceleration region in Hall Thruster

IEPC-2019-880

Presented at the 36th International Electric Propulsion Conference
University of Vienna • Vienna, Austria
September 15-20, 2019

L. Nicole[1], P. Sarrailh[2] and M. Villemant[3]
ONERA - The French Aerospace Lab, Toulouse, France

L. Garrigues[4]
LAPLACE, Université de Toulouse, CNRS, Toulouse, France

and

C. Boniface[5]
CNES - French National Space Agency, Toulouse, France

Abstract: Hall Thrusters is a technology of interest for space industry due to its use for electric orbit rising. Nonetheless, Hall Thruster plasma behavior is not fully understood today. Among other topics, the modelling of electron transport in Hall Thruster channel is still an issue. In this article, the interaction between Hall Thruster plasma and channel wall through electron emission is studied for the acceleration region of the Hall Thruster. To do so, a Particle-In-Cell simulation of acceleration region including a detailed electron emission model is used. Preliminary results of this study indicate that electron emission can not explain the major part of electron transport in the acceleration region.

Nomenclature

ϵ_0 = Vacuum dielectric permittivity ($\epsilon_0 = 8.85 \cdot 10^{-12}\ F.m^{-1}$)
σ = Total electron emission yield [∅]
δ = Secondary electron emission yield [∅]
η_e = Elastically backscattered electron emission yield [∅]
η_i = Inelastically backscattered electron emission yield [∅]
w_f = Material work function$[eV]$
θ_0 = Incident electron angle to the surface normal $[rad]$
θ = Incident electron deviation angle$[eV]$
α = Emitted electron angle to the wall $[rad]$
φ = Emitted electron precession angle $[eV]$
Γ_0 = Flux of incident electrons to the wall $[m^{-2}.s^{-1}]$
Γ_{se} = Flux of emitted secondary electrons $[m^{-2}.s^{-1}]$

[1] Ph.D. student, Department Physics, Instrumentation, Environment, Space (DPHY), lucas.nicole@onera.fr
[2] Research Scientist, Department Physics, Instrumentation, Environment, Space (DPHY), pierre.sarrailh@onera.fr
[3] Research Scientist, Department Physics, Instrumentation, Environment, Space (DPHY), marc.villemant@onera.fr
[4] Senior Scientist at CNRS, GREPHE group, laurent.garrigues@laplace.univ-tlse.fr
[5] Dr, electric propulsion R&T manager, Propulsion, Pyrotechnics and Aerothermodynamics section, Claude.Boniface@cnes.fr

Γ_{eb} = Flux of elastically backscattered electrons $[m^{-2}.s^{-1}]$
σ_i = Flux of inelastically backscattered electrons $[m^{-2}.s^{-1}]$
σ_e = Flux of inelastically backscattered electrons $[m^{-2}.s^{-1}]$
$d\Omega$ = Flux of inelastically backscattered electrons $[m^{-2}.s^{-1}]$
E_e = Emitted electron energy $[eV]$
E_0 = Incident electron energy $[eV]$

SLAB = Single Large Angle Backscattering
PIC = Particle In Cell

I. Hall Thruster technology and its impact on space industry

PLASMA propulsion for satellites presents a significant industrial growth thanks to its propulsive efficiency (17 000 m/s of exhaust velocity for Hall thruster in particular) and its reliability. This technology allows major cost saving due to the reduction of the needed mass of exhaust gas (from several thousands of kilograms to some dozen of kilograms). Satellites integrators are already commercializing all electric propulsion satellites (i.e. satellites only propelled with plasma thrusters). Hall thrusters are today the most common plasma thruster type for the electric orbit rising of telecommunication satellites. Nonetheless, it is impossible today to predictively model the Hall thrusters plasma behavior as well as the influence of physical parameters on it. Consequently, it is difficult to optimize the Hall thrusters wall material, their dimensions, etc. Thus, the understanding of Hall thruster plasma physics is today a major concern for space industry.

II. Acceleration zone modelling description

A. Particle-In-Cell/Monte-Carlo Collisions modelling method

The non-maxwellian nature of charged particle species in a Hall thruster makes the use of Particle-In-Cell techniques suitable to characterize the plasma properties [1], [2]. Particle-In-Cell (PIC) method combines an Eulerian approach to calculate electromagnetic field properties and Lagragian techniques by sampling the unknown distribution functions with a fixed number of macroparticles. Motions of macroparticles are integrated in phase space by solving the equations of trajectories. In Hall thrusters, solely electrons are magnetized and only the applied magnetic field affects the electron transport. The self-induced magnetic field by the Hall current in the azimuthal direction is negligible. The electric field induced by space charge is calculated solving Poisson equation on a prescribed grid whose cell size (Δx) must be shorted than the electron Debye length in the explicit version of PIC technique. Using a time step (Δt) smaller than a fraction of the electron plasma frequency avoids the particles at thermal velocity to cross more than one cell during one timestep. Collisions between electrons and neutrals are tackled with a Monte Carlo module based on the null collision technique [3].

Typical number of particles are between 100 and 500 per-cell, and with the typical conditions of HT operations, these give $\Delta x < 30$ μm and $\Delta t < 5 \times 10^{-12}$ s.

B. Electron emission modelling in PIC simulation

Electron emission is the result of three phenomena: secondary electron emission, elastic backscattering and inelastic backscattering. Secondary electron emission is the ejection of electron due to ionization process under the impact of incident electrons. Most of the secondary electrons are emitted in the vacuum with an energy of a few eV. Elastic backscattering is the reemission of incident electrons which only endured elastic collisions in the material. They reemerge in the vacuum with an energy equal to the incident energy (E_0). Inelastic backscattering is the reemission in the vacuum of incident electrons which encountered at least one inelastic collision in the material. They reemerged in the vacuum with an energy lower than E_0. The secondary electron emission yield (noted δ) is the ratio of the emitted secondary electron flux ($\Gamma_{\mathrm{se}}[m^{-2}.s^{-1}]$) on the incident electron flux (Γ_0 $[m^{-2}.s^{-1}]$, cf. Fig.1.a). Elastically backscattered electron emission yield (noted η_e) is the flux of elastically backscattered electrons ($\Gamma_{eb}[m^{-2}.s^{-1}]$) on the incident electron flux (cf. Fig.1.b). Finally, the inelastically backscattered electron yield (noted η_i) is the flux of inelastically backscattered electron ($\Gamma_{ib}[m^{-2}.s^{-1}]$) on the incident electron flux (cf. Fig.1.c). Experimentally, inelastically backscattered electrons are difficult to distinguish from secondary electrons especially at low incident electron energy ($E_0 \leq 20\ eV$). Nonetheless, it is possible to identify some contributions of inelastically backscattered electrons to the emitted electron energy spectrum, such as volume and surface plasmons

peaks [4]. Besides, it should be noted that inelastically backscattered electrons are often neglected or confused with the secondary electrons in plasma modelling. Nonetheless some empirical models of inelastically backscattered electron exist [5] and were used in plasma modelling without determining if their influence on simulations results were determining or negligible [6].

The sum of these three terms is the total electron emission yield (noted σ):

$$\sigma = \delta + \eta_e + \eta_i = \frac{\Gamma_{\mathrm{se}}}{\Gamma_0} + \frac{\Gamma_{\mathrm{eb}}}{\Gamma_0} + \frac{\Gamma_{\mathrm{ib}}}{\Gamma_0}$$

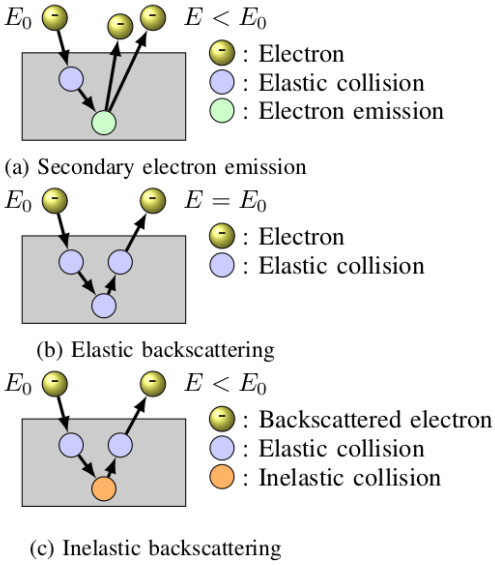

Figure 1 : Electron emission phenomenon, breakdown between secondary electron emission, elastic backscattering and inelastic backscattering

To have a detailed description of EE, it is needed to describe it in term of yield, angular distribution and energy distribution for the three populations of electrons (secondary electrons, elastically backscattered electrons and inelastically backscattered electrons). In order to do so, three models from literature are used. SEEY is described according to Vaughan model [7], secondary electrons energy distribution is described by Chung and Everheart's model [8] and elastically backscattered electrons angular distribution is described by the single large angle backscattering (SLAB) model [9]. By definition, elastically backscattered electrons are emitted with an energy equal to the incident electron energy (E_0) and secondary electrons are often considered with a isotropic angular distribution. Finally, in this model inelastically backscattered electrons are neglected. The detailed model properties are described in Table I.

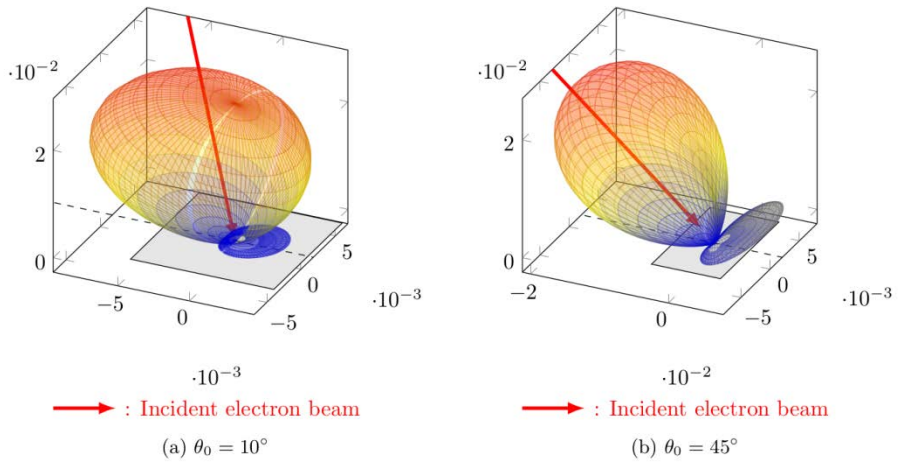

(a) $\theta_0 = 10°$ (b) $\theta_0 = 45°$

Figure 2 : Elastic backscattering lobes for an aluminium surface with an incident electron energy $E_0 = 40\ eV$ and two different incident angle: $\theta_0 = 10$ ° (a) and $\theta_0 = 45$ ° (b).

Chung and Everheart's model gives an analytical description of secondary electron energy distribution, which only depends on material work function (w_f).

$$\frac{dN_e}{dE_e} = 6w_f^4 \frac{E_e}{(E_e + w_f)^6}$$
$$\langle E_e \rangle = 2w_f$$

The single large angle backscattering (SLAB) model is based on the idea that the emission direction of an elastically backscattered electron is driven by a main interaction giving the deviation angle and that the probability of emission can be averaged on all elastic and inelastic collisions probability along the electron trajectory. These hypotheses allow obtaining the following expression of the differential solid angle elastic backscattering yield:

$$\frac{d\eta_e}{d\Omega} = \frac{\cos(\alpha)}{\cos(\alpha) + \cos(\theta_0)} \left(\frac{1}{\sigma_e}\frac{d\sigma_e}{d\Omega}\right)(\theta) \ln\left(1 + \frac{\sigma_e}{\sigma_i}\right)$$

With θ_0 $[rad]$ the incident electron angle to surface normal, α $[rad]$ the elastically backscattered electron angle to the surface normal, θ $[rad]$ the deviation angle of the backscattered electron, σ_e $[nm^2]$ the elastic collision cross section, σ_i $[nm^2]$ the inelastic collision cross section and $d\Omega$ $[srad]$ the considered solid angle of emission. θ is given by:

$$\theta = \arccos[\sin(\theta_0)\sin(\alpha)\cos(\varphi) - \cos(\theta_0)\sin(\alpha)]$$

A representation of EBEY depending on emission angle is plotted on Fig.2. It can be noticed on this figure that angular distribution of elastically backscattered is far from being isotropic, which is a current assumption. Besides it is highly dependent on incident electron angle (θ_0) and incident electron energy (E_0).

Vaughan's model [7] was created to fit experimental TEEY with only three parameters: the maximum value of TEEY ($\sigma_{\max}$), the incident electron energy at this value ($E_{\max}$) and a curvature parameter (k). As Vaughan model has been created to fit TEEY experimental data at high incident electron energy ($E_0 > 1\ keV$), where the overwhelming part of the emitted electrons are secondary electrons, it has been chosen to fit SEEY only with Vaughan model. To do so, $\sigma_{\max}$ and $E_{\max}$ are firstly evaluated according to experimental data, then $\eta_{e,max} = \eta_e(E_{\max})$ is calculated according to SLAB model. Finally $\delta_{\max}$ is evaluated by neglecting inelastically backscattered electrons:

$$\delta_{\max} = \sigma_{\max} - \eta_{e,\max}$$

All the values of δ can then be calculating according to Vaughan's model:

$$\delta(E_0, \theta_0) = \delta_{\max}(E_0, \theta_0)\left[v(E_0, \theta_0)\exp\left(1 - v(E_0, \theta_0)\right)\right]^k$$

This model allows taking into account the dependency of SEEY to incident angle according to:

$$v(E_0, \theta_0) = \frac{E_0}{E_{0,\max}(\theta_0)}$$

$$E_{0,\max}(\theta_0) = E_{0,\max}(\theta_0 = 0)\left(1 + \frac{k_s}{\pi}\theta_0^2\right)$$

$$\delta_{\max}(\theta_0) = \delta_{\max}(\theta_0 = 0)\left(1 + \frac{k_s}{2\pi}\theta_0^2\right)$$

With k_s the material surface state parameter (by default $k_s = 1$).

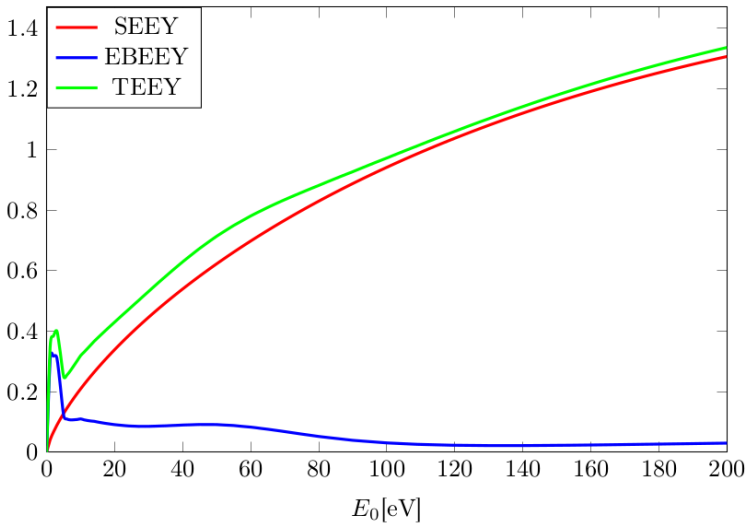

Figure 3 : Total electron emission yield (TEEY) and breakdown between secondary electron emission yield (SEEY) and elastically backscattered electron emission yield (EBEEY) as a function of incident electron energy (E_0) for an incident electron beam normal to the surface ($\theta_0 = 0$ °)

C. Acceleration zone boundary conditions

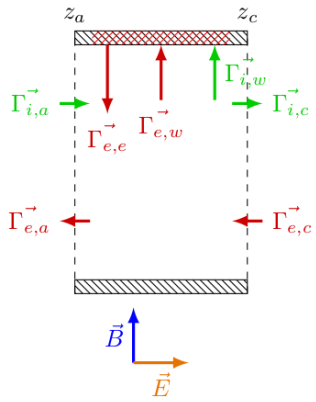

Figure 4 : Ion and electron balance at acceleration region boundary

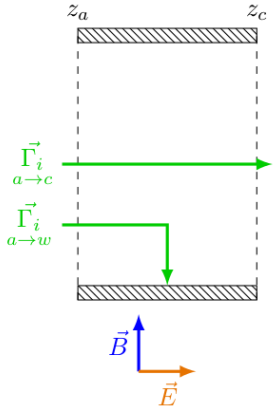

Figure 5 : Ion balance in acceleration region

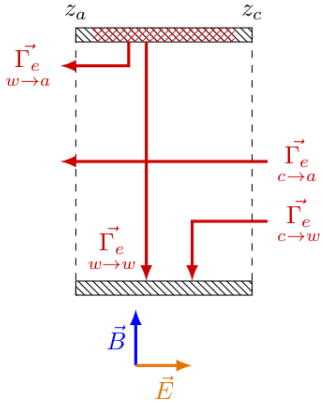

Figure 6 : Electron balance in acceleration region

In the acceleration zone, the boundary conditions are chosen to respect the particle conservation and therefore, the electro-neutrality outside of the sheath. The figures 3, 4 and 5 represent a slice of the annular thruster in the radial – axial plan, with, at the bottom, the inner wall and at the top, the outer wall. The exhaust plan is at the right

and the end of the ionization zone at the left. When an ion and an electron leave the domain, the pair is injected back at a same random radial position but the electron at the cathode and the ion at the exit of the ionization zone.

D. 1.5D modelling

To study the axial transport of the electrons in the channel, it is necessary to add an axial dimension to the 1D-radial simulation. However, by the choice of cutting the thruster in two zones of constant axial electric field, radial magnetic field and considering that the whole ionization takes place in the ionization zone, it is possible to study the electron transport without solving Poisson' equation in the axial direction.

III. Collision model influence on axial electron mobility in acceleration region

The acceleration zone reveals lack of electron transport in the axial direction. The ions are indeed accelerated by a constant axial electrical field and are non magnetized but the electrons are trapped in the constant radial magnetic field and only move thanks to collisions. Nonetheless ions and electrons must have the same mobility in the thruster as the ion and electron currents are equal. This implies the existence of an additional electron mobility. As the latter is not fully understood today, it is qualified as abnormal electron mobility. To simulate the abnormal mobility in the acceleration region and maintain the electron transport in the channel an abnormal electron collision frequency is needed because the elastic and wall collisions are not sufficient to explain the movement of electrons.
To add collisions that represent an azimuthal wave, an abnormal neutral density was added, which induces elastic collisions but only in the axial/azimuthal plan, like instabilities in the Hall thruster. To respect the physics while enhancing the transport, a value of $n_{ab} = 5 \cdot 10^{18}\ m^{-3}$ is appliqued. Table 1 presents a physical set of data used, which is representative of the order of magnitude involved in a Hall thruster:

Axial electrical field	27000	V/m
Radial magnetic field	200	G
Plasma density	$1{,}56 \cdot 10^{18}$	m^{-3}
Neutral density	10^{18}	m^{-3}
Radial length	$2 \cdot 10^{-2}$	m
Axial length	$7{,}5 \cdot 10^{-3}$	m

Table 1 Input data for the PIC simulation

Figure 7 shows the electron and ion densities (respectively red and blue curves) at the end of the simulation ($t_f = 80\mu s$). On the same figure, the final radial electric potential is plotted (green curve). It can be observed that the electro-neutrality is respected in plasma center. Indeed, electron and ion density curves are superimposed and a constant plasma potential around $80\ V$ is observed. At the boundaries of the plasma, a strong decrease of electron and ion density can be observed. Besides, a dropping of electron density compared to ion density can also be observed. This difference between electron and ion densities next to the wall induces a strong increase of electric potential from $0V$ at the wall to the plasma potential at the center of the channel ($\varphi_p \simeq 80\ V$).

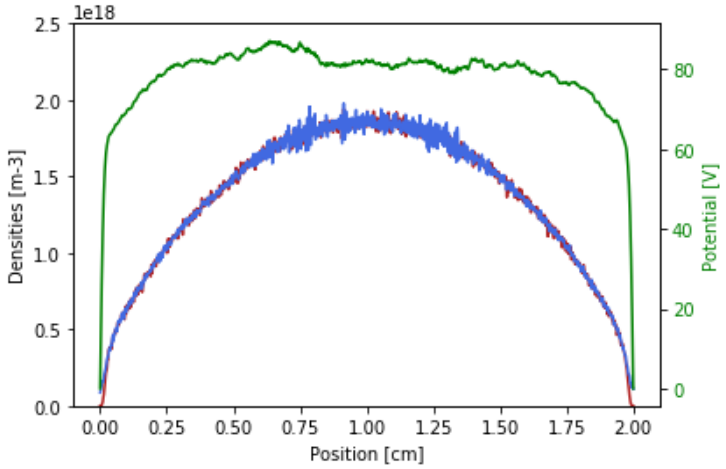

Figure 7 Density profile and potential for Table 1 data

	$n_{ab} = 5 \cdot 10^{18} m^{-3}$			$n_n = 1.0 \cdot 10^{18} m^{-3}$		
	Anode	Cathode	Walls	Anode	Cathode	Walls
Electrons current [A/m²]	117,40	0,50	5,73	19,50	1,24	85,27
Ions current [A/m²]	0,00	1908,50	315,74	0,00	1306,16	134,19

Table 2 Current by species at the boundaries

The addition of the abnormal collision term leads to a fit of summed PIC collision frequency to theoretical frequency calculated by theses two ways:

$$\upsilon = \frac{e \cdot B^2 \cdot v_{axiale}}{m_e \cdot E} = \frac{e \cdot B \cdot v_{axiale}}{m_e \cdot v_{azimuthale}}$$

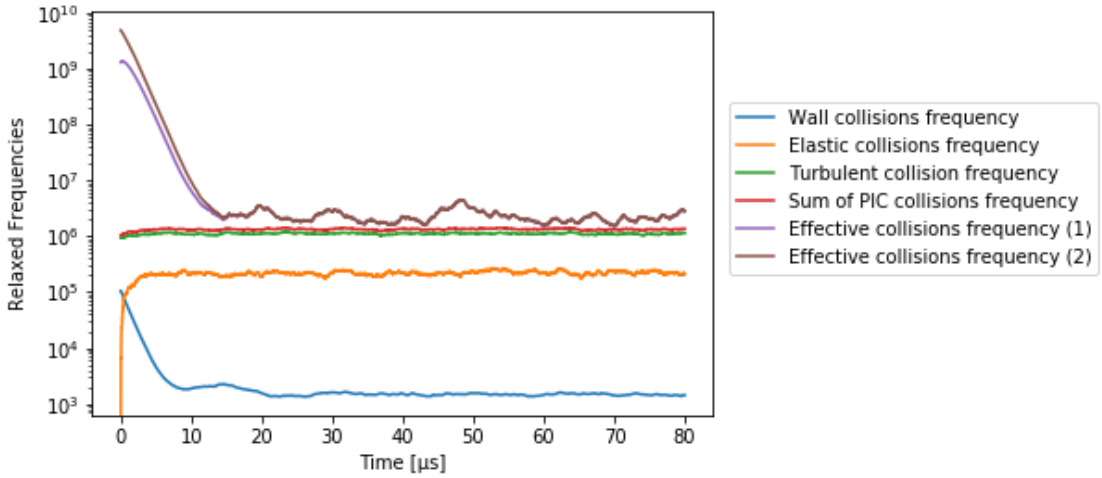

Figure 8 Collisions frequencies for Table 1 Data

Figure 9 shows the influence of the abnormal density on the electron current to the ionization zone ($I_{e,IZ}$). It can be observed that the increase of n_{ab} induces of the electron current to the ionization zone from $I_{e,IZ} = 40\ A/m^2$ for $n_{ab} = 1.0 \cdot 10^{18}\mathrm{m}^{-3}$ to $I_{e,IZ} = 250\ A/m^2$ for $n_{ab} = 1.0 \cdot 10^{18}\mathrm{m}^{-3}$.

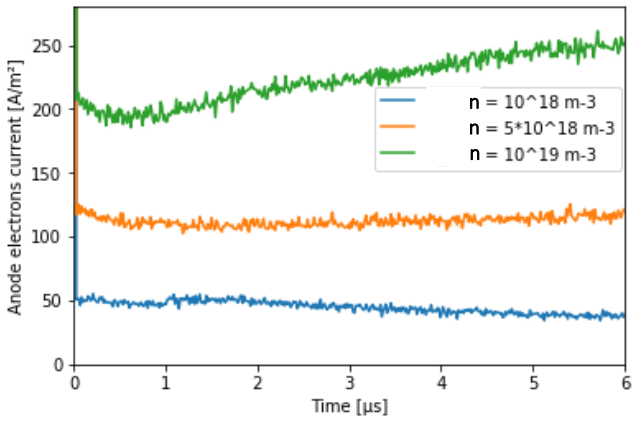

Figure 9 Current of electrons at the end of the ionization zone for several values of turbulent density

A parametrical study let us determine that $n_{ab} = 5 \cdot 10^{18} m^{-3}$ allows keeping a constant number of macro-particles in the simulation while keeping, in the meantime, realistic values for the plasma potential ($\varphi_p \simeq 80$ V as presented in Figure 7).

As a standard set of simulation parameters has been determined (i.e. Table 1 and $n_{ab} = 5 \cdot 10^{18} m^{-3}$), the influence of electron emission at the channel wall will now be studied based on this preliminary study.

IV. Electron emission influence on axial electron mobility in acceleration region

In this section, the influence of electron emission on electron current toward the ionization region is studied. More precisely, three criteria have been taken into account : the model of electron emission, the model of secondary electron energy distribution and the model elastically backscattered electron angular distribution.

Figure 10 shows the electrons current to the ionization region as a function of simulation time without electron emission (orange curve) and with electron emission simulated according to Barral model (blue curve). It can be observed that the electron emission model seems to have no effect on electron current to the ionization region. Figure 11 shows the electrons current to the ionization region as a function of simulation time without electron emission and for three angular distribution models of elastically backscattered electrons. As the four curves are superimposed, it can be consider that the chosen angular model has no influence on electron mobility in the acceleration region. Figure 12 shows the electrons current to the ionization region as a function of simulation time without electron emission and for two secondary electron energy distribution models. As the three curves are superimposed, it can be consider that the secondary electron energy distribution has no significant influence on electron mobility in the acceleration region.

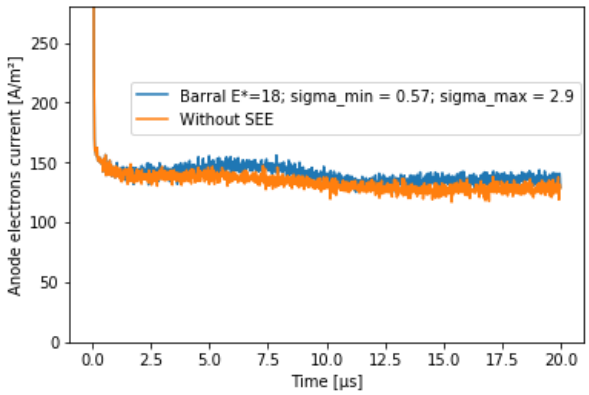

Figure 10 : Anode electron current as a function of simulation time without electron emission (orange curve) and with secondary electron emission according to Barral's model [10].

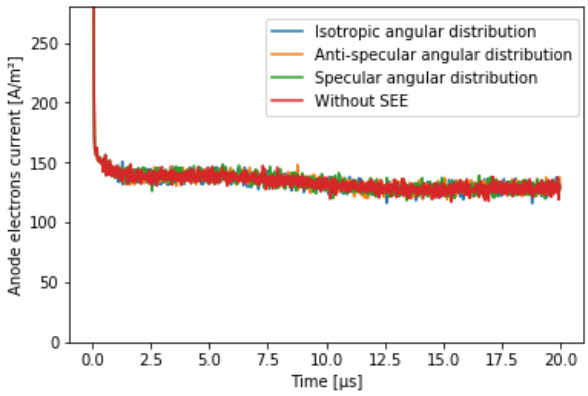

Figure 11 : Anode electron current as a function of simulation time for four models of electron emission angular distribution.

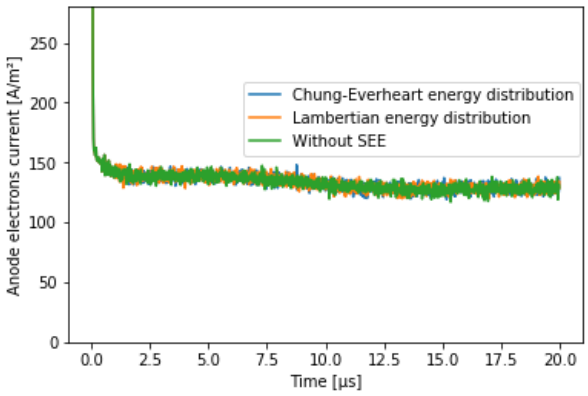

Figure 12 : Anode electron current as a function of simulation time for three models of secondary electron energy distribution.

V. Conclusion and further studies

The current results show a negligible influence of electron emission on electron axial transport in the acceleration region, even when realistic secondary electron energy distribution and emitted electron angular distributions are taken into account. This seems to indicate that another physical phenomenon has to be considered to explain the axial electron transport throughout the acceleration region. Among other hypotheses, the electron-cyclotron drift instability (ECDI) could have a major influence on electron transport.

Nonetheless several improvements could still be performed on the current PIC code. First of all, until now the dielectric properties of the channel walls are not considered. To do so an electric capacitance could be imposed at the wall boundaries (as done by Domínguez-Vázquez et al. [11]). Besides there is currently no numerical condition to ensure the axial current conservation. Indeed, in steady state the axial ion current toward the channel exhaust should equal the axial electron current to the ionization region. A fluid condition could be imposed to adapt axial electric current to the disequilibrium between axial electron current and axial ion current. Finally, it could be interesting to fix a total electron mobility of the electron and to adapt the empirical abnormal mobility to the electron mobility due to the interaction between the electrons and the wall. This could give us a quantitative analysis of the electron emission contribution to the electrons transport.

References

[1] R. W. Hockney and J. W. Eastwood, *Computer Simulation Using Particles*. CRC Press, 1988.

[2] C. K. Birdsall and A. B. Langdon, *Plasma Physics via Computer Simulation*. CRC Press, 2004.
[3] V. Vahedi and M. Surendra, "A Monte Carlo collision model for the particle-in-cell method: applications to argon and oxygen discharges," *Computer Physics Communications*, vol. 87, no. 1, pp. 179–198, May 1995.
[4] J. Pierron, C. Inguimbert, M. Belhaj, T. Gineste, J. Puech, and M. Raine, "Electron emission yield for low energy electrons: Monte Carlo simulation and experimental comparison for Al, Ag, and Si," *Journal of Applied Physics*, vol. 121, no. 21, p. 215107, Jun. 2017.
[5] D. Sydorenko, "Particle-in-cell simulations of electron dynamics in low pressure discharges with magnetic fields," University of Saskatchewan Saskatoon, 2006.
[6] D. Sydorenko, A. Smolyakov, I. Kaganovich, and Y. Raitses, "Modification of electron velocity distribution in bounded plasmas by secondary electron emission," *Plasma Science, IEEE Transactions on*, vol. 34, pp. 815–824, Jul. 2006.
[7] J. R. M. Vaughan, "A new formula for secondary emission yield," *IEEE Transactions on Electron Devices*, vol. 36, no. 9, pp. 1963–1967, Sep. 1989.
[8] M. S. Chung and T. E. Everhart, "Simple calculation of energy distribution of low-energy secondary electrons emitted from metals under electron bombardment," *Journal of Applied Physics*, vol. 45, no. 2, pp. 707–709, Feb. 1974.
[9] A. Jablonski, "Angular distribution of elastic electron backscattering from surfaces: determination of the electron inelastic mean free path," *J. Phys. D: Appl. Phys.*, vol. 47, no. 5, p. 055301, 2014.
[10] S. Barral, K. Makowski, Z. Peradzyński, N. Gascon, and M. Dudeck, "Wall material effects in stationary plasma thrusters. II. Near-wall and in-wall conductivity," *Physics of Plasmas (1994-present)*, vol. 10, no. 10, pp. 4137–4152, Oct. 2003.
[11] A. Domínguez-Vázquez, F. Taccogna, and E. Ahedo, "Particle modeling of radial electron dynamics in a controlled discharge of a Hall thruster," *Plasma Sources Sci. Technol.*, vol. 27, no. 6, p. 064006, Jun. 2018.